



Atomic structure of nanoscale quasicrystal-forming Zr–noble metal binary metallic glasses

J. Saida^{a,*}, K. Itoh^b, T. Sanada^c, S. Sato^d, M. Imafuku^e, M. Ohnuma^f, A. Inoue^g

^a Center for Interdisciplinary Research, Tohoku University, Aramaki Aoba, Aoba-ku, Sendai 980-8578, Japan

^b Graduate School of Education, Okayama University, Tsushimanaka, Kita-ku, Okayama 700-8530, Japan

^c Research Department, Nissan ARC Ltd., Natsushima, Yokosuka 237-0061, Japan

^d Institute for Materials Research, Tohoku University, Katahira, Aoba-ku, Sendai 980-8577, Japan

^e Faculty of Engineering, Tokyo City University, Setagaya-ku, Tokyo 158-8557, Japan

^f National Institute of Materials Science (NIMS), Sengen, Tsukuba, Ibaraki 305-0047, Japan

^g WPI-AIMR, Tohoku University, Katahira, Aoba-ku, Sendai 980-8577, Japan

ARTICLE INFO

Article history:

Received 1 July 2010

Received in revised form 9 December 2010

Accepted 14 December 2010

Available online 21 December 2010

Keywords:

Metallic glasses

Quasicrystallization

Local structure

Simulation

Zirconium-based alloy

ABSTRACT

We report the results of the local structural evaluation and mechanism of QC formation in the $Zr_{70}Pd_{30}$ and $Zr_{80}Pt_{20}$ glassy alloys. Voronoi analysis indicates the difference of local environment between two alloys. The perfect icosahedron frequently exists around Zr atom and major polyhedra have prism-like structure around Pd in $Zr_{70}Pd_{30}$. In contrast, icosahedral-like distorted polyhedra formation is favorable around Pt as well as Zr in $Zr_{80}Pt_{20}$. It is therefore, concluded that the quasicrystallization originates from the medium-range order based on the Zr-centered perfect icosahedron and the Pd-centered prism-like ones remain during the QC phase formation in $Zr_{70}Pd_{30}$. Icosahedral-like local structure around Zr and Pt might contribute together to the nucleation of QC phase in $Zr_{80}Pt_{20}$. This feature with a different mechanism of QC formation in the two alloys may correlate to the difference of solute concentration and the structure of stable crystalline phase after the decomposition of QC phase.

© 2010 Elsevier B.V. All rights reserved.

1. Introduction

It has been well known that local structure investigation is quite important to understand the mechanism of high glass-forming ability (GFA) in metallic glasses [1]. Several studies on the primary nanoscale quasicrystallization in Zr–Al–Ni–Cu multi-component metallic glasses by the additional elements [2–4] or oxygen impurity [5,6] have led us to new aspects of the local structure characterization in the glassy state. That is, the primary nano icosahedral quasicrystalline phase (I-phase) formation exhibits the possibility of a common environment between the I-phase and local atomic configuration in the glassy state [7]. Actually, we have already reported the local structural similarity between the glassy and quasicrystal (QC)-formed states in the Zr–Al–Ni metallic glass [8]. Based on the series of such studies, we have clarified that the stability of supercooled liquid state, *i.e.*, GFA strongly correlates with the formation of icosahedral local structure in Zr-based glassy alloys [7,9]. The suggestion has been also supported by the several simulation studies [10,11]. However, the transformation mecha-

nism of the I-phase from the glassy state has not been still cleared due to the difficulty of local structure evaluation in multicomponent alloy systems.

Recently, simple QC-forming glassy alloys such as ternary and binary systems in Zr–Cu–NM (NM: noble metal) and Zr–(Pd or Pt) have been proposed [9,12–14]. The results may indicate the formation of icosahedral local structure in corresponding ternary and binary systems as well as multicomponent metallic glasses with a stable supercooled liquid state. Especially, Zr–(Pd and Pt) binary metallic glasses enable us to evaluate the local structure between the glassy and QC-formed states in detail, which is expected to clarify the mechanism of quasicrystallization from the viewpoint in the atomic structure around the each constitutional element. Actually, Takagi *et al.*, have preliminary reported a considerable icosahedral clusters around Zr atom in the as-quenched state and the increase of them during QC precipitation in the $Zr_{70}Pd_{30}$ metallic glass using the electron diffraction structure analysis [15]. It leads to a speculation of the growth of nano I-phase originating from the quenched-in icosahedral clusters around Zr atom. In this paper, we investigate the nano quasicrystallization process and the detailed structure analysis on the local environment in the $Zr_{70}Pd_{30}$ and $Zr_{80}Pt_{20}$ metallic glasses by small angle X-ray scattering (SAXS), radial distribution function (RDF) analyses and X-ray absorption fine structure (EXAFS) studies. On the basis of these experimental results, we

* Corresponding author. Tel.: +81 22 795 5752; fax: +81 22 795 5756.
E-mail address: jsaida@cir.tohoku.ac.jp (J. Saida).

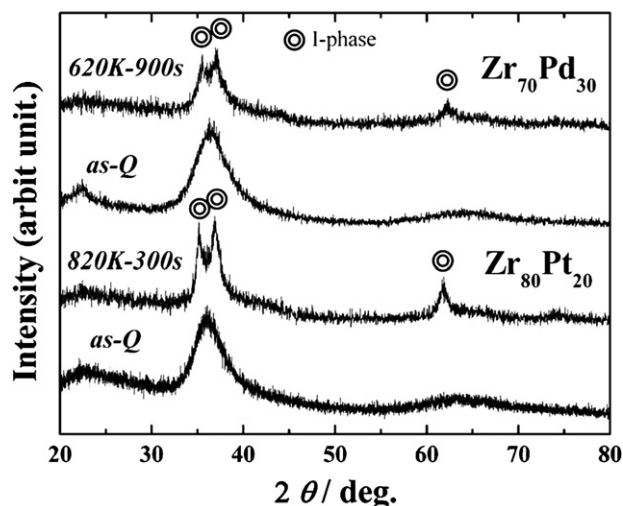


Fig. 1. X-ray diffraction (XRD) patterns of the $Zr_{70}Pd_{30}$ and $Zr_{80}Pt_{20}$ alloy ribbons in the as-quenched and annealed states.

have adopted the simulation approach with a reverse Monte Carlo (RMC) method and Voronoi polyhedral analysis in order to identify the clusters involved in QC formation. Moreover, we also intend to compare the QC forming process between the two binary alloys.

2. Experimental procedures

The glassy ribbon samples were prepared by single roller melt quenching for the master alloys of $Zr_{70}Pd_{30}$ and $Zr_{80}Pt_{20}$ produced by arc-melting high purity metals of 99.9 mass% Zr, 99.9 mass% Pd and 99.98 mass% Pt in a purified argon atmosphere. The samples were annealed in a vacuum atmosphere. The as-quenched and annealed structure was examined by transmission electron microscopy (TEM) in addition to the X-ray diffractometry (XRD) analysis with Cu-K α radiation at 40 kV to 40 mA. The samples for TEM observation were prepared by the ion milling technique. The precipitation process of the QC phase was analyzed by small-angle X-ray scattering (SAXS). We used a high-flux/high-transmission Mo-K α ($\lambda = 0.07$ nm) SAXS system with a two-dimensional con-focal mirror (Rigaku Nano-viewer) and a two-dimensional detector (Bruker High-star) measured in the Q -region from 0.2 to 10 nm^{-1} . The local atomic structures were studied by ordinary X-ray diffraction measurements with monochromatic Mo-K α radiation of 50 kV to 300 mA produced by a rotating anode X-ray generator. The scattered X-ray intensities were corrected for air-scattering, absorption, polar-

ization effects and converted to electron units per atom by the generalized Krogh–Moe–Norman method to obtain a structure factor, $S(Q)$ [16]. EXAFS measurements for the analysis of local environment around Zr, Pd and Pt atoms were performed at SPring-8 synchrotron radiation on beam line BL01B1. All measurements were done in transmission geometry at room temperature. Measured spectra were analyzed using the program REX 2000 (Rigaku Corp.). The EXAFS simulation of each structure model was performed using the FEFF 8.2 code [17].

RMC simulations were carried out through fitting to the X-ray structure factor in the range of $Q = 10\text{--}150\text{ nm}^{-1}$. Starting configuration of 5000 atoms with an appropriate composition, randomly distributed in a cubic box of length 4.6889 nm for $Zr_{70}Pd_{30}$ and 4.7689 nm for $Zr_{80}Pt_{20}$, was used. The r -spacing of the partial pair correlation functions was set to 0.01 nm. To ensure a physically realistic configuration, the closest distances between two atoms were determined to be 0.28 nm for Zr–Zr, 0.25 nm for Zr–Pd and Zr–Pt, 0.24 nm for Pd–Pd and 0.28 nm for Pt–Pt based on the results of our preliminary study of radial distribution functions (RDFs) [18,19]. Voronoi polyhedral analysis was performed on the RMC configurations. First-coordination-shell distances were determined from the minimum positions in the partial pair correlation functions.

3. Results and discussion

3.1. Precipitation and growth of nano QC phase

Fig. 1 shows X-ray diffraction (XRD) patterns of the $Zr_{70}Pd_{30}$ and $Zr_{80}Pt_{20}$ alloy ribbons in the as-quenched and annealed states. Annealing conditions are 620 K – 900 s for $Zr_{70}Pd_{30}$ and 820 K – 300 s for $Zr_{80}Pt_{20}$. No significant XRD peaks except a halo peak are observed in the as-quenched state in both alloys. In contrast, all the diffraction peaks in both the annealed alloys can be identified as an icosahedral quasicrystalline phase (I-phase). Typical high-resolution TEM images of the as-quenched and annealed (820 K – 300 s) $Zr_{80}Pt_{20}$ alloy are shown in **Fig. 2(a)** and **(c)**, respectively. Homogeneous maze-like pattern without any significant contrast corresponding to an ordered region is obtained in the HREM image of the as-quenched alloy. The selected-area electron diffraction pattern (SADP) in **Fig. 2(b)** contains only a halo ring, which is consistent with the HREM image and XRD result. Fine particle with a diameter around 20 nm is homogeneously distributed in the glassy matrix in the annealed sample in **(c)**. A typical fast Fourier transformation (FFT) pattern from the precipitated particles shown in **Fig. 2(d)** clearly indicates the fivefold symmetry, which reveals the transformation from glassy to I-phase. We have already reported the transformation processes of the $Zr_{70}Pd_{30}$ and $Zr_{80}Pt_{20}$ metallic

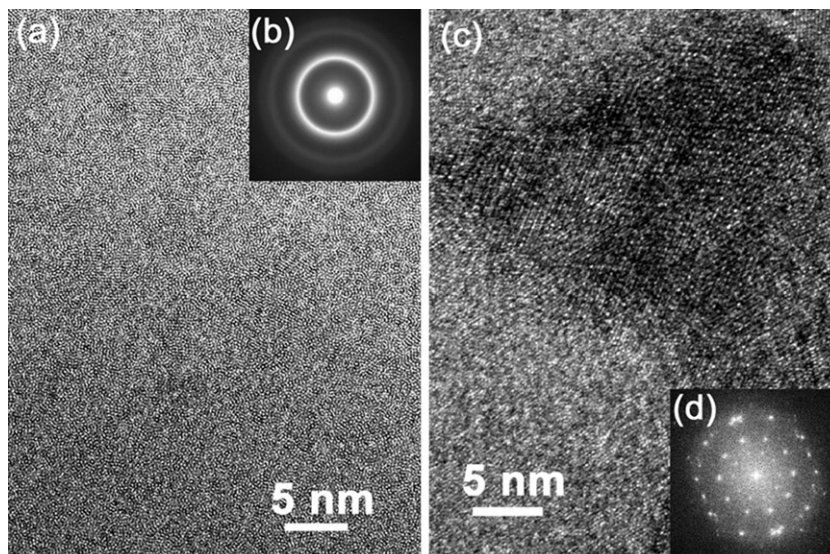


Fig. 2. Typical high-resolution TEM images of the as-quenched (a) and annealed (820 K – 300 s) (c) $Zr_{80}Pt_{20}$ alloy. (b) Selected-area electron diffraction pattern (SADP) in the as-quenched state. (d) Fast Fourier transformation (FFT) pattern from the precipitated particles in (c).

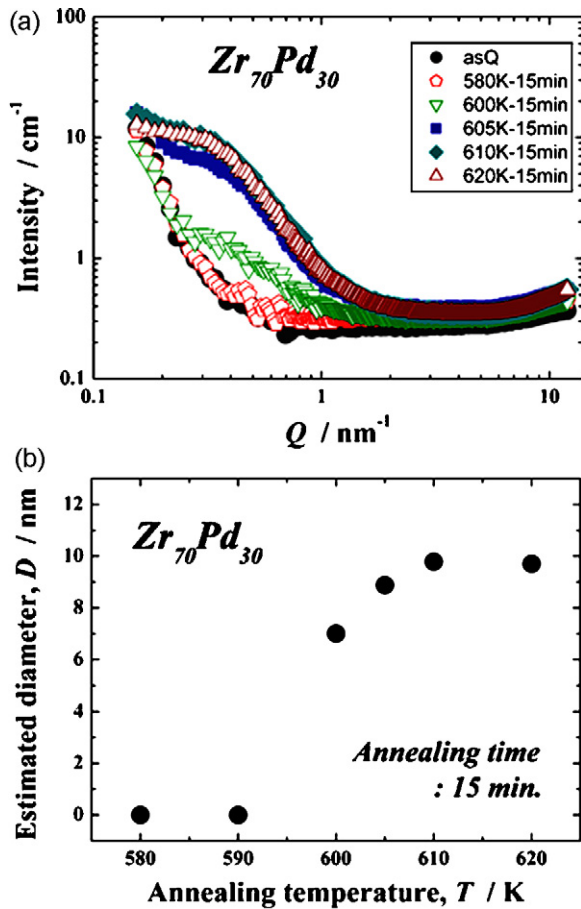


Fig. 3. (a) SAXS profiles of the $Zr_{70}Pd_{30}$ metallic glass in the as-quenched and annealed states. (b) Plots of the diameter estimated by the Guinier approximation for various annealing temperatures.

glasses in the isochronal annealing of the heating rate of around 0.67 K/s as follows [20];

Glassyphase \rightarrow I- + glassy(minor)phases \rightarrow Zr_2Pd : $Zr_{70}Pd_{30}$

Glassyphase \rightarrow I- + glassy(minor)phases

\rightarrow Zr + ZrPt + Zr_5Pt_3 + Zr_9Pt_{11} : $Zr_{80}Pt_{20}$

The difference of the final intermetallic compounds between two alloys may imply the different formation or growth mechanism of QC phase.

The SAXS profiles of the $Zr_{70}Pd_{30}$ metallic glass in the as-quenched and annealed states are shown in Fig. 3(a). The annealing has been performed for 15 min at temperatures ranging from 580 to 620 K in the vacuum atmosphere. Since we have already reported the distribution of constitutional elements during the QC precipitation [20], it can be detected easily by SAXS measurement. The intensity of the sample after annealing at the temperatures over 600 K becomes stronger in the entire $Q (=4\pi \sin \theta / \lambda, \lambda$: wave length) region than that in the as-quenched one. Fig. 3(b) shows the plots of the diameter estimated by the Guinier approximation for various annealing temperatures. Here, the diameter of “0” reveals the homogeneous glassy structure. The QC phase is detected at 600 K in the SAXS profile without any obvious precursors, in which the size is calculated to be approximately 7 nm in diameter. The result indicates that the QC phase appears abruptly at the onset quasicrystalline temperature. We speculate the nucleation and growth of QC phase by cooperative-like motion of several atoms, *i.e.*, by rearranging the several icosahedral ordered regions or clusters in

Table 1

Calculated nearest neighbor atomic distances, r and coordination numbers, N from XRD measurements in the $Zr_{70}Pd_{30}$ and $Zr_{80}Pt_{20}$ glassy alloys.

	Pairs	r (nm)	N
$Zr_{70}Pd_{30}$	Zr–Zr	0.326 ± 0.002	8.3 ± 0.4
	Zr–Pd	0.289 ± 0.001	3.7 ± 0.2
	(Pd–Zr)		8.6 ± 0.2
	Pd–Pd	0.273 ± 0.002	0.6 ± 0.2
$Zr_{80}Pt_{20}$	Zr–Zr	0.326 ± 0.002	8.8 ± 0.3
	Zr–Pt	0.286 ± 0.001	2.3 ± 0.2
	(Pt–Zr)		9.3 ± 0.2
	Pt–Pt	0.326 ± 0.002	1.8 ± 0.2

the initial stage without a diffusion of individual atoms. The QC phase grows up to 10 nm in diameter and further grain growth is not confirmed at the higher annealing temperatures, which is also consistent to the suggestion above. Namely, it is thought that very fine grain size originates from the many icosahedral medium-range orders as nucleation sites and the saturation of grain size exhibits the growth caused by arranging the related icosahedral clusters around the center core (*i.e.*, icosahedral cluster origin-cooperative motion), in which the individual atoms do not diffuse for QC growing. In such case, the QC particles have to stop to grow after possible and related clusters have already aggregated. It is due to the stable clusters originating from the strong chemical affinity between Zr and noble metal. The investigation described above has been strongly suggested in the recent studies [10,21,22]. Mechler et al. [21] have reported that QC grows from the undercooled liquid more likely by the attachment of performed icosahedral clusters, rather than by a single atom attachment in the local structure studies in Zr–Ti–Ni–Cu metallic glass. The simulation study has also pointed out that icosahedral clusters would like to “wet” the core of the QC nucleus owing to the reduction of interfacial tension. These clusters change the connectivity to ordered QC arrangements as the nucleus grows. Actually, we have already clarified the QC growth involving the icosahedral ordered regions by the high-resolution TEM observation in the present $Zr_{70}Pd_{30}$ metallic glass [23].

3.2. Local structure characterization

Fig. 4(a) and (b) shows the experimental structure factors, $S(Q)$, obtained by XRD measurements (solid line) and RMC fitting (broken line) for the $Zr_{70}Pd_{30}$ and $Zr_{80}Pt_{20}$ glassy alloys, respectively. Partial structure factors, $S_{ij}(Q)$, derived from the RMC model are also shown in Fig. 4(c) ($Zr_{70}Pd_{30}$) and (d) ($Zr_{80}Pt_{20}$). Since $S(Q)$ obtained from the RMC model is in excellent agreement with the experimental results of XRD measurements in both alloys, we can verify the validity of RMC modeling. A significant prepeak around $Q \sim 17 \text{ nm}^{-1}$ is observed in $Zr_{80}Pt_{20}$ as shown in Fig. 4(b). It is suggested that the prepeak is attributed to the unique bonding between the Pt–Pt pair, as can be verified by the corresponding partial structure factors, $S_{ij}(Q)$. This feature leads to the existence of a strong chemical short- or medium-range order around the Pt atom as displayed in Fig. 4(d) [24]. The $Zr_{70}Pd_{30}$ alloy does not have any prepeaks significantly in total $S(Q)$, however, slight one is also characterized in the partial structure factors, $S_{ij}(Q)$ of the Pd–Pd pair (Fig. 4(c)). The total and partial pair distribution functions, $g(r)$ and $g_{i-j}(r)$, respectively for the $Zr_{70}Pd_{30}$ and $Zr_{80}Pt_{20}$ glassy alloys calculated from the RMC models are shown in Fig. 5(a) and (b), respectively. The position of the first peak is estimated to be at 0.31 nm for Zr–Zr, 0.28 nm for Zr–Pd, 0.28 nm for Pd–Pd in $Zr_{70}Pd_{30}$ and 0.31 nm for Zr–Zr, 0.28 nm for Zr–Pt, 0.33 nm for Pt–Pt in $Zr_{80}Pt_{20}$. These results are reasonably consistent with those obtained from the RDF analysis in previous reports as shown in Table 1 [15,18,24,25]. The intensity of the second peak in the Pt–Pt pair is relatively high, which may be reflected by the prepeak observed at $Q \sim 17 \text{ nm}^{-1}$ in $S(Q)$. Similar high inten-

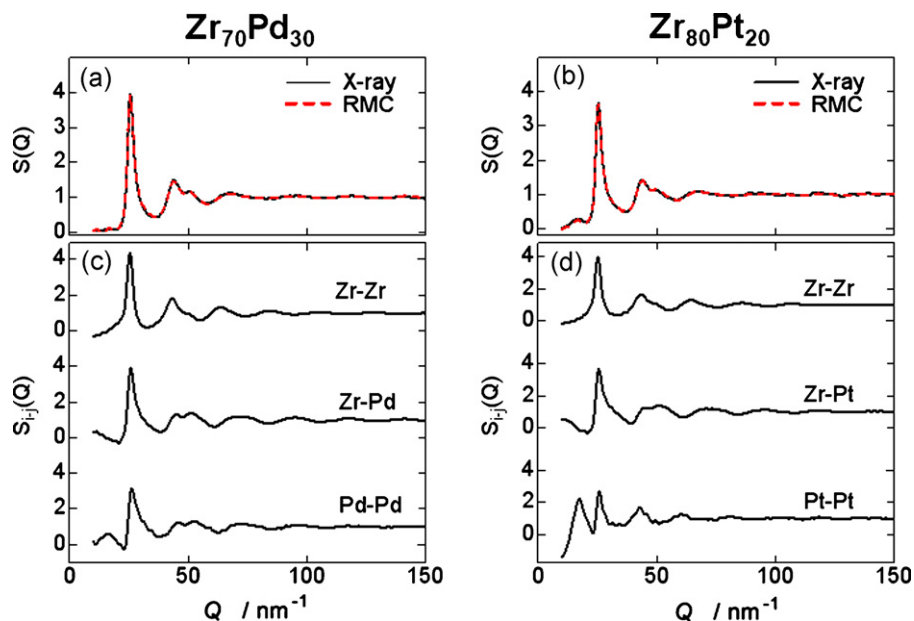


Fig. 4. Experimental structure factors, $S(Q)$, obtained by XRD measurements (solid line) and RMC fitting (broken line) for the $\text{Zr}_{70}\text{Pd}_{30}$ (a) and $\text{Zr}_{80}\text{Pt}_{20}$ (b) glassy alloys. Partial structure factors, $S_{ij}(Q)$, derived from the RMC model of $\text{Zr}_{70}\text{Pd}_{30}$ (c) and $\text{Zr}_{80}\text{Pt}_{20}$ (d).

sity of the second peak in the Pd–Pd pair is also observed, however it is a little bit comparing to that of the Pt–Pt pair. We speculate that the correlation in relatively longer distance of the Pd and Pt atoms might imply the formation of large cluster with the second or third shell, or medium-range scale atomic configuration comprising several clusters. Actually, similar prepeak has been also reported in the QC-forming Al–Fe–Ce molten alloy, in which the estimated size of the structure unit is approximately 0.45 nm in diameter [26]. The size of unit is almost equivalent to that of the single icosahedron. The correlation length (*i.e.*, cluster size) of such short-range order (single icosahedron) increases with decreasing temperature of liquid or glass-forming. Consequently, the cluster size is evaluated to be 1.6–2.0 nm in diameter in the glassy solid. Here, it is noted that the structural unit size still remains unchanged.

The result indicates that the cluster is constituted by 6–10 icosahedral structural units (short-range orders) fused together via vertex, edge or plane sharing. It is suggested that this atomic structure exhibits the correlation in considerably longer distance and such cluster is simultaneously a candidate of nucleus of the QC phase.

In order to examine the local environment around Zr, Pd and Pt atoms, we performed EXAFS measurements for the glassy and QC-formed states of the $\text{Zr}_{70}\text{Pd}_{30}$ and $\text{Zr}_{80}\text{Pt}_{20}$ alloys. The Fourier transformation curves of EXAFS measurements of the Zr K-edge (a), Pd K-edge (b) and Pt L3-edge (c) in the in the $\text{Zr}_{70}\text{Pd}_{30}$ and $\text{Zr}_{80}\text{Pt}_{20}$ alloys in the glassy and annealed (QC-formed) states are shown in Fig. 6. The local environment around Zr in the QC-formed state slightly differs from that in the as-quenched state in the

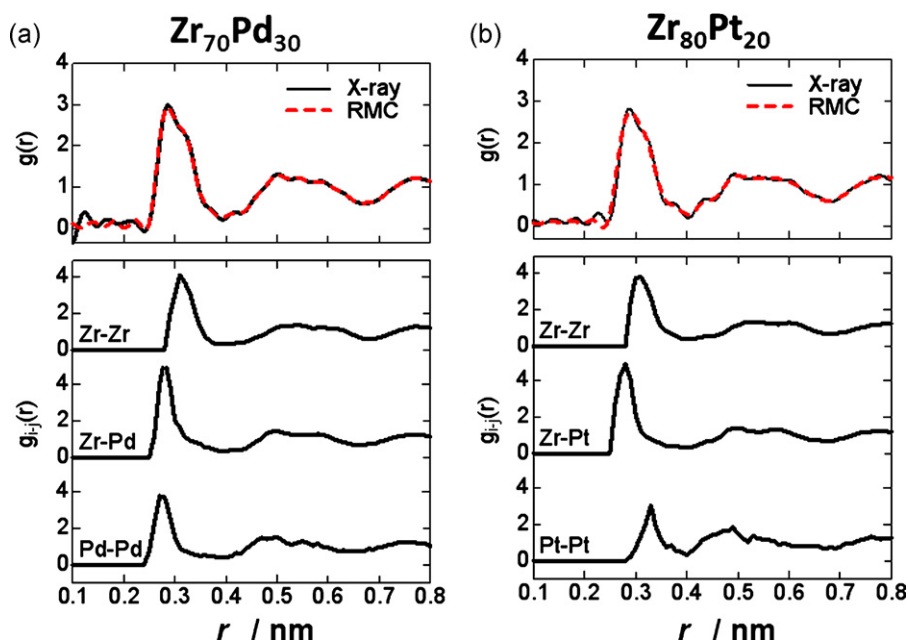


Fig. 5. Total and partial pair distribution functions, $g(r)$ and $g_{ij}(r)$, respectively, calculated from the RMC models for the $\text{Zr}_{70}\text{Pd}_{30}$ (a) and $\text{Zr}_{80}\text{Pt}_{20}$ (b) glassy alloys. The results of $g(r)$ from XRD measurements are also denoted.

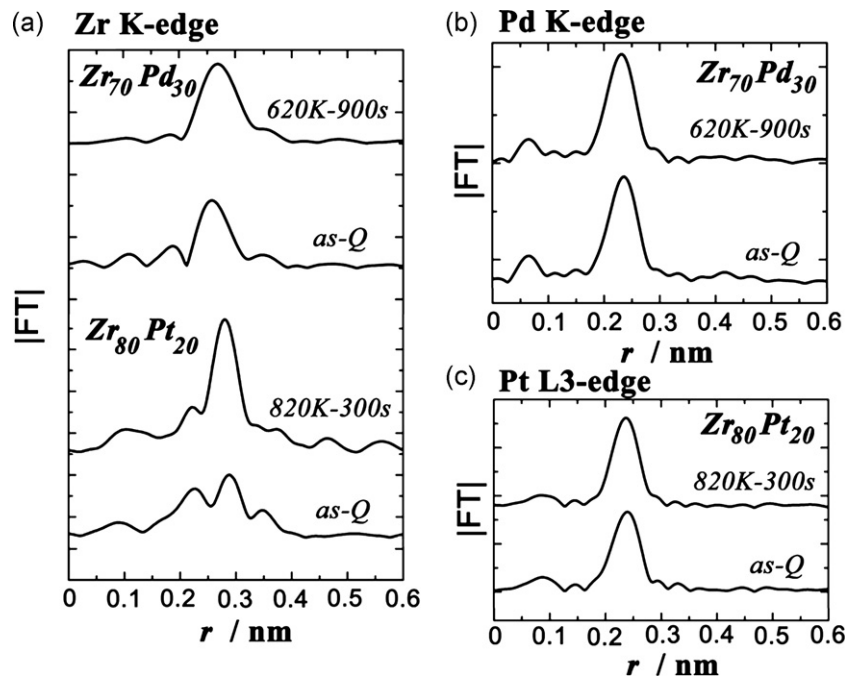


Fig. 6. Fourier transformation curves of EXAFS measurements of the Zr K-edge (a), Pd K-edge (b) and Pt L3-edge (c) in the $Zr_{70}Pd_{30}$ and $Zr_{80}Pt_{20}$ alloys in the glassy and annealed (QC-formed) states.

$Zr_{70}Pd_{30}$ alloy, however, local environment changes significantly during quasicrystallization in $Zr_{80}Pt_{20}$ alloy. In contrast, the Fourier transformation curves of the Pd and Pt edges in the as-quenched and QC-formed states resemble each other in both alloys, indicating that the local environment does not change through the quasicrystallization. It is therefore suggested that the QC formation proceeds with a rearrangement of atoms around Zr and it is distinguished more in $Zr_{80}Pt_{20}$.

3.3. QC formation and growth processes in Zr–noble metal binary alloys

As we mentioned, a number of studies have pointed out that the QC formation strongly correlates to the presence of icosahedral local structure in the glassy state. Although we have to consider the different scale length between the local cluster and QC nucleus, several papers have suggested the model or mechanism of QC nucleation in correlation with the icosahedral local structure [10,22,26–29]. These studies allow us to examine the number and/or stability of icosahedral local structure for clarifying the mechanism of the QC formation effectively in the present alloys. Based on the RMC results as shown in Figs. 4 and 5, the local structure around Zr, Pd and Pt atoms is examined using Voronoi polyhedral analysis of the preferential structure models. Fig. 7 shows the fractions of Voronoi polyhedra around Zr (a) and Pd (b) atoms in the $Zr_{70}Pd_{30}$ and Zr (c) and Pt (d) atoms in the $Zr_{80}Pt_{20}$ glassy alloys. Here, the polyhedra of perfect icosahedral, icosahedral-like (distorted) and prism-like are denoted by red, green and blue colors, respectively. The dominant formation of polyhedra of icosahedral family such as (0, 2, 8, 2), (0, 2, 8, 1), (0, 1, 10, 2), (0, 0, 12, 0) and (0, 3, 6, 3), are observed around the Zr atom in $Zr_{70}Pd_{30}$ (Fig. 7(a)), which are generally consistent with those in the previous study using X-ray and electron diffraction measurements [15,17]. In contrast, prism and prism-like local environments (blue color) with the indices of (0,3,6,0), (0,3,6,1), (0,2,8,0) and (0,4,4,0) mainly exist around the Pd atom as shown in Fig. 7(b). Since these polyhedra strongly correlate to the stable Zr_2Pd crystalline phase, it may remain until the decom-

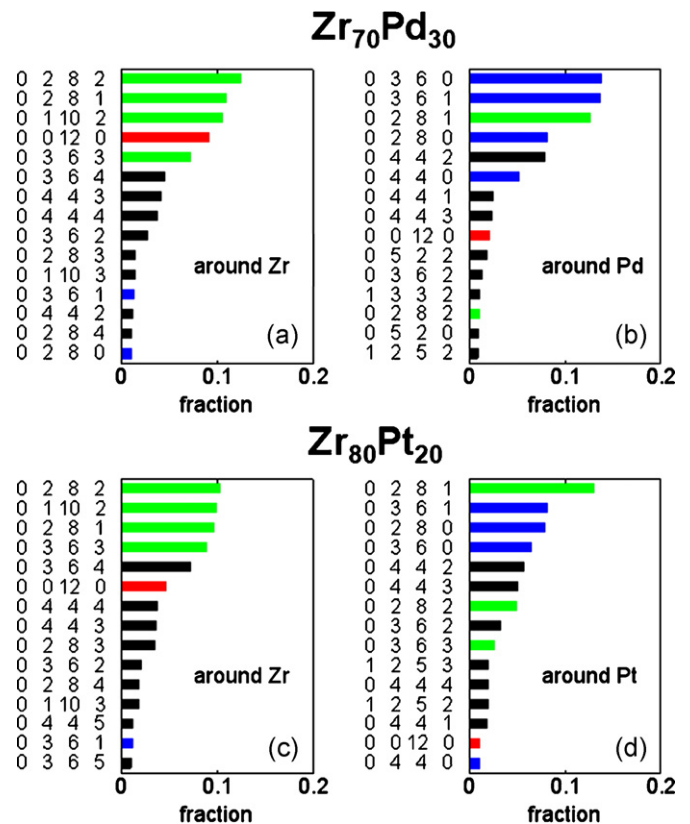


Fig. 7. Fractions of Voronoi polyhedra around Zr (a) and Pd (b) atoms in the $Zr_{70}Pd_{30}$ and Zr (c) and Pt (d) atoms in the $Zr_{80}Pt_{20}$ glassy alloys. Here, the polyhedra of perfect icosahedral, icosahedral-like (distorted) and prism-like are denoted by red, green and blue colors, respectively. (For interpretation of the references to color in this figure legend, the reader is referred to the web version of the article.)

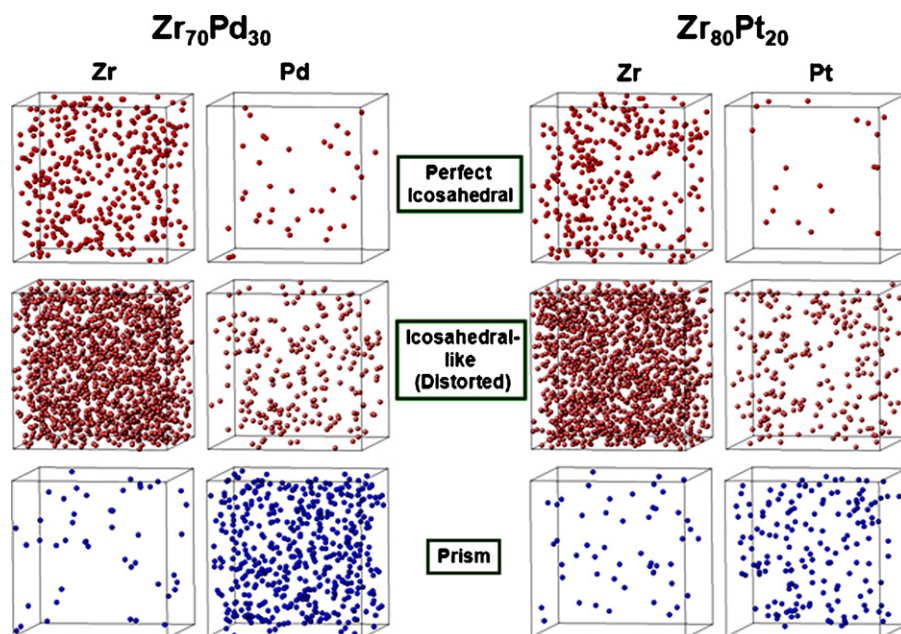


Fig. 8. Distribution of icosahedral, icosahedral-like (distorted) and prism polyhedra around Zr, Pd and Pt atoms.

position of QC phase. The investigation is consistent with the results of EXAFS measurements, which indicate that local environment around the Pd atom does not change significantly during the precipitation of the I-phase. Subsequently, it is also reasonable, when we consider that the QC phase has a Pd-poor composition [20].

In $Zr_{80}Pt_{20}$, the fraction of icosahedral-like polyhedra (green color) such as (0,2,8,2), (0,1,10,2), (0,2,8,1) and (0,3,6,3) with the coordination numbers of 11–13, is relatively high around the Zr atom. However, the perfect icosahedron (red color) with a Voronoi index of (0,0,12,0) appears less frequently than that in $Zr_{70}Pd_{30}$. These results are interpreted that the distorted icosahedral local structure is formed around the Zr atom in the alloy. Additionally, polyhedra with higher coordination numbers such as (0,2,8,4), (0,1,10,3) and (0,3,6,5) are frequently observed, which may be in correlation with a Zr_5Pt_3 -like structure. In contrast, the Voronoi polyhedron with an index of (0,2,8,1) with icosahedral-like geometry is dominant around the Pt atom as shown in Fig. 7(d). It has also been investigated by an *ab initio* molecular dynamics simulation [30]. Since this polyhedron simultaneously corresponds to the local environment around Pt in the Zr_5Pt_3 crystalline phase [31], it may be thermodynamically stable through the entire transformation processes from glass to QC and from QC to Zr_5Pt_3 plus others. Actually, the EXAFS results with unchanged local environment around Pt atom during the precipitation of the I-phase are obtained.

In order to investigate the mechanism of QC formation in both alloys, we visualize the distribution of icosahedral, icosahedral-like (distorted) and prism polyhedra around Zr, Pd and Pt atoms as shown in Fig. 8. Each dot reveals the center atom of the corresponding polyhedra. As described above, the perfect icosahedral atomic configuration as well as the distorted one is formed more frequently around Zr atom in $Zr_{70}Pd_{30}$. Few polyhedra belonging to the icosahedral family are observed around Pd. These results lead to the conclusion that the I-phase originates from the Zr-centered icosahedral atomic structure. In $Zr_{80}Pt_{20}$, icosahedral-like atomic configurations are characterized around Pt atom as well as Zr atom, even though the perfect one contains less comparing to that in $Zr_{70}Pd_{30}$. It is therefore, concluded that the I-phase can be formed from both atoms.

According to these investigations, a different mechanism of QC formation for the two binary alloys is suggested. In the Zr–Pd binary alloy, the origin of QC phase is the icosahedral local order with considerably more ordered geometry around the Zr atom. Such order may be stabilized thermodynamically with Pd-centered prism-like ones, which correlate to the structure of stable Zr_2Pd phase. These ordered clusters might be related to the strong chemical affinity between Pd and Zr. Meanwhile, several icosahedral-like local orders around Pt atom as well as around Zr atom contribute together to the QC formation in the $Zr_{80}Pt_{20}$ glassy alloy. We have already reported that the QC phase can be formed directly from the melt of $Zr_{80}Pt_{20}$ by cooling at an appropriate rate [32]. Since similar phenomenon is not observed in the $Zr_{70}Pd_{30}$ glassy alloy, we can point out that the $Zr_{80}Pt_{20}$ glassy alloy has a tendency to form the icosahedral-like environment around both Zr and Pt atoms. Especially, dominant icosahedral-like local environment not the prism-like one around Pt, which strongly correlates to the Zr_5Pt_3 stable phase, leads to the easy growth of the QC phase without any significant rearrangement of the constitutional elements [20]. The results of our investigation are also supported by the previous study that the I-phase can precipitate with a low activation energy [33]. It should be also suggested that such difference of local environment between two alloys might originate from the difference of the concentration of solute elements [34]. The solute atom fraction generally contributes to the state of packing, bond formation and free volume introduction. These are the important factors of the definition of local environment in the glassy structure. The lower solute content in Zr–Pt alloy leads to the less contact of Pt–Pt, which results in the formation of local environment consisting of Zr–Pt. It also brings the longer pair distance of Pt–Pt, comparing to that of the Pd–Pd pair in Zr–Pd alloy.

Finally, we investigate the growth mechanism of QC in the present alloys. As described in the previous paragraph, the QC phase grows from the icosahedral cluster-origin (cooperative motion of several icosahedral clusters), not by the individual atomic diffusion. Based on the suggestion as well as the local environmental change examined by EXAFS, growth mechanism in both alloys is summarized as follows. In the $Zr_{70}Pd_{30}$ alloy, the QC phase initially nucleates from the icosahedral medium-range order based on the Zr-centered perfect icosahedron attached by the several

icosahedral clusters around it and grows by a rearrangement of related clusters. During the QC growth, Zr (~5 at.%) is enriched, which brings a slight change of local environment around Zr, indicating that partial Zr element might play a role as glue atom among the clusters. Pd-centered prism like clusters almost remain during the QC formation, however they are considerably rejected from the QC phase. In the $Zr_{80}Pt_{20}$ alloy, the QC phase can nucleate from the icosahedral medium-range order around the both atoms and the distortion of icosahedral clusters requires the rearrangement of atoms for QC growing. Especially, since the approximately 40% Zr_5Pt_3 -like local environment exists with major icosahedral one around the Zr atom [19], it is necessary to rearrange the Zr atom more for the QC growth. The major Pt-centered local clusters with icosahedral-like geometry might result in the relatively unchanged local environment during the QC nucleation and growth.

4. Conclusions

In the present study, we reported the results of the local structural evaluation and the mechanism of QC formation and growth in the $Zr_{70}Pd_{30}$ and $Zr_{80}Pt_{20}$ glassy alloys. We observed that the QC phase precipitates with no obvious precursors upon annealing, of which origin is recognized as the quenched-in icosahedral local structure. Actually, many icosahedrons are detected in the glassy state in both alloys. However, Voronoi analysis clearly indicates the difference of the distribution of them between two alloys. The perfect icosahedron exists more around Zr atom in $Zr_{70}Pd_{30}$, comparing to that in $Zr_{80}Pt_{20}$. Although, major polyhedra are prism-like structure around Pd in $Zr_{70}Pd_{30}$, some icosahedral-like polyhedra and few prism-like ones are also investigated around Pt in $Zr_{80}Pt_{20}$. It is therefore, concluded that the different QC formation and growth mechanism is suggested. That is, the quasicrystallization originates from the icosahedral medium-range order based on the Zr-centered perfect icosahedron and the Pd-centered prism-like ones remains until the decomposition of QC phase in $Zr_{70}Pd_{30}$. In contrast, icosahedral-like local structure around Pt as well as Zr might contribute to the nucleation of QC phase in $Zr_{80}Pt_{20}$. This feature with a different mechanism of QC formation in the two alloys may also correlate to the difference of solute concentration and the structure of stable crystalline phase.

Acknowledgements

This work is supported by Grant-in-Aid of the Ministry of Education, Sports, Culture, Science and Technology, Japan, Scientific

Research (A) and Priority Area on “Science and Technology of Microwave-Induced, Thermally Non-Equilibrium Reaction Fields”.

References

- [1] D.B. Miracle, T. Egami, K.M. Flores, K.F. Kelton, *MRS Bull.* 32 (2007) 629–634.
- [2] M.W. Chen, T. Zhang, A. Inoue, A. Sakai, T. Sakurai, *Appl. Phys. Lett.* 75 (1999) 1697–1699.
- [3] L.Q. Xing, J. Eckert, W. Löser, L. Schultz, *Appl. Phys. Lett.* 74 (1999) 664–666.
- [4] J. Saida, A. Inoue, *J. Phys. Condens. Matter* 13 (2001) L73–L78.
- [5] J. Eckert, N. Mattern, M. Zinkevitch, M. Seidel, *Mater. Trans. JIM* 39 (1998) 623–632.
- [6] U. Köster, A. Rüdiger, J. Meinhardt, *Mater. Sci. Forum* 307 (1999) 9–16.
- [7] J. Saida, C. Li, M. Matsushita, A. Inoue, *J. Mater. Res.* 16 (2001) 3389–3401.
- [8] J. Saida, M. Imafuku, S. Sato, T. Sanada, E. Matsubara, A. Inoue, *Philos. Mag. Lett.* 85 (2005) 135–144.
- [9] J. Saida, E. Matsubara, A. Inoue, *Mater. Trans.* 44 (2003) 1971–1977.
- [10] H. Tanaka, *J. Phys. Condens. Matter* 15 (2003) L491–L498.
- [11] D.B. Miracle, A.L. Greer, K.F. Kelton, *J. Non-Cryst. Solids* 354 (2008) 4049–4055.
- [12] B.S. Murty, D.H. Ping, K. Hono, *Appl. Phys. Lett.* 77 (2000) 1102–1104.
- [13] J. Saida, M. Matsushita, A. Inoue, *Appl. Phys. Lett.* 77 (2000) 73–75.
- [14] D.J. Sordelet, X.Y. Yang, E.A. Rozhkova, M.F. Besser, M.J. Kramer, *Appl. Phys. Lett.* 83 (2003) 69–71.
- [15] T. Takagi, T. Ohkubo, Y. Hirotsu, B.S. Murty, K. Hono, D. Shindo, *Appl. Phys. Lett.* 79 (2001) 485–487.
- [16] C.N.J. Wagner, H. Ocken, M.L. Joshi, *Z. Naturforsch.* 20a (1965) 325–335.
- [17] A.L. Ankudinov, B. Ravel, J.J. Rehr, S.D. Conradson, *Phys. Rev. B* 58 (1998) 7565–7576.
- [18] M. Imafuku, J. Saida, A. Inoue, *J. Mater. Res.* 11 (2001) 3046–3049.
- [19] J. Saida, T. Sanada, S. Sato, M. Imafuku, A. Inoue, *Appl. Phys. Lett.* 91 (2007) 111901-1–111901-3.
- [20] J. Saida, M. Matsushita, A. Inoue, *J. Appl. Phys.* 90 (2001) 4717–4724.
- [21] S. Mechler, G. Schumacher, V. Koteski, H. Riesemeier, F. Schäfers, H.E. Mahnke, *Appl. Phys. Lett.* 97 (2010) 041914-1–041914-3.
- [22] A.S. Keys, S.C. Glotzer, *Phys. Rev. Lett.* 99 (2007) 235503-1–235503-4.
- [23] J. Saida, M. Matsushita, A. Inoue, *Appl. Phys. Lett.* 79 (2001) 412–414.
- [24] M. Kitada, M. Imafuku, J. Saida, A. Inoue, *J. Non-Cryst. Solids* 312–314 (2002) 594–598.
- [25] J. Saida, T. Sanada, S. Sato, M. Imafuku, C. Li, A. Inoue, *Z. Kristallogr.* 223 (2008) 726–730.
- [26] L. Zhang, Y. Wu, X. Bian, H. Li, W. Wang, J. Lin, N. Lun, *J. Phys. Condens. Matter* 11 (1999) 7959–7969.
- [27] A.P. Tsai, *Sci. Technol. Adv. Mater.* 9 (2008) 013008-1–013008-20.
- [28] L. Yang, J.Z. Jiang, T. Liu, T.D. Hu, T. Uruga, *Appl. Phys. Lett.* 87 (2005) 061918-1–061918-3.
- [29] P.J. Steinhardt, *Mater. Sci. Eng. A* 294–296 (2000) 205–210.
- [30] D.J. Sordelet, R.T. Ott, M.Z. Li, S.Y. Wang, C.Z. Wang, M.F. Besser, A.C.Y. Liu, M.J. Kramer, *Metall. Mater. Trans. A* 39 (2008) 1908–1916.
- [31] E. Matsubara, T. Nakamura, M. Sakurai, M. Imafuku, S. Sato, J. Saida, A. Inoue, *Mater. Res. Soc. Proc.* 644 (2001) L1.1.1.1–L1.1.1.12.
- [32] J. Saida, M. Matsushita, A. Inoue, *Mater. Trans.* 42 (2001) 1103–1108.
- [33] M.H. Lee, R.T. Ott, M.F. Besser, M.J. Kramer, D.J. Sordelet, *Scripta Mater.* 55 (2006) 505–508.
- [34] D.B. Miracle, D.V. Louzguine-Luzgin, L.V. Louzguina-Luzgina, A. Inoue, *Int. Mater. Rev.* 55 (2010) 218–256.